Low-Temperature Geothermal Play Fairway Analysis for the Denver Basin

Estefanny Davalos Elizondo[1], Nicole Taverna[1], Abra Gold[1]

[1]National Renewable Energy Laboratory, Golden, CO

Keywords

Denver Basin, Play Fairway Analysis, Geothermal Direct Use, Combined Heat and Power, Sedimentary Basin Geothermal Play Type, Python Code, Favorability Map

ABSTRACT

This project is part of a national initiative to showcase the benefits of incorporating low-temperature geothermal resource assessment into the deployment of geothermal heating, combined heat and power (CHP), and geothermal direct-use (GDU) technologies. The initiative was established to accelerate the country's decarbonization efforts by identifying potential for low-temperature geothermal resource utilization (<150°C, e.g., CHP and GDU) in selected sedimentary basins with numerous population centers.

The play fairway analysis (PFA) methodologies in this study were adapted from previous PFA investigations of sedimentary basin geothermal play types (SBGPTs) that evaluated the potential for low-temperature resources (<150°C). Workflows, relevant datasets, a new Python library, and common and composite geological criteria maps are utilized to develop low-temperature geothermal resource favorability maps for the Denver Basin, a sedimentary basin spanning Colorado, Nebraska, and Wyoming. The replication of these methodologies in other SBGPTs can evaluate potential for low-temperature resources. To facilitate future assessment of low-temperature geothermal resources in SBGPTs, this project provides PFA workflows, data, tools, and favorability maps that will ultimately support the utilization of low-temperature geothermal resources in sedimentary basins.

1. Introduction

Sedimentary basins often have numerous layers of highly porous rocks and can have elevated fracture permeability, depending on the stress regimes affecting each basin. Candidate fluids for low-temperature geothermal utilization (<150°C) readily accumulate in these naturally porous, fractured rocks at depth. Nearly half of the United States is underlain by sedimentary basins that have been widely uninvestigated for low-temperature geothermal resource potential (USGS 2022).

A sedimentary basin geothermal play type (SBGPT) is influenced by its historical development and current tectonic and geological conditions. Crucial elements of an SBGPT include heat sources, the presence of circulating fluids (either natural or injected) for heat transport, reservoir porosity and permeability as well as storage attributes (both natural and induced), and reservoir

seals. These characteristics differ from hydrocarbon play systems, which are characterized by their source rock, reservoir traps, and trapping mechanisms (Doughty et al. 2018).

Most hydrothermal plays dominated by conduction in sedimentary basins occur in deep aquifers with a nearly normal thermal gradient (Moeck 2014). Variations in porosity and permeability are dictated by lithology, faulting, diagenetic patterns, and stress fields (Wolfgramm et al. 2009; Hartmann and Beaumont 2000), all of which are significantly shaped by the evolution, subsidence rates, and contemporary tectonics. Previous research focusing on geothermal resources in sedimentary formations emphasized those with high porosity/high permeability (~100 mD) for effective convection (Augustine 2014) or high porosity/low permeability at elevated temperature gradients, typically found at depths greater than 3 km (Moeck 2014). SBGPTs with low permeability may harbor petrothermal resources, which can be accessed by enhancing permeability through various reservoir stimulation techniques (Zimmermann et al. 2007). The storage capacity related to the host rock's porosity could critically affect the performance of Enhanced Geothermal Systems (EGS) in hot sedimentary aquifers (Rybach 1981).

It is imperative that more research be conducted to evaluate the potential for low-temperature geothermal resources in highly permeable and porous rocks of sedimentary basin geothermal play types (SBGPTs). This study centers on implementing a geothermal play fairway analysis (PFA), adapted from the hydrocarbon industry for low-temperature resources in SBGPTs, with a specific focus on the Denver Basin. The workflow is based on the forthcoming Geothermal Play Fairway Analysis Best Practices report (Pauling et al. 2023) and the Low-Temperature Geothermal Play Types assessment (Davalos-Elizondo et al. 2023), which identified a general geothermal PFA process (Figure 1).

PFA methodologies should be adapted to each geothermal play type individually. To classify this SBGPT, we used the scheme suggested by Coleman and Cahan (2012) based on a simple geological setting (Figure 2): (1) intracratonic basins created within the boundaries of a craton; (2) pericratonic basins formed near or accreted to the margins of the craton; (3) intercratonic basins formed between cratons and extend onto oceanic crust; and (4) oceanic basins that developed independently of cratons, primarily on oceanic crust.

Identification of areas with low-temperature geothermal potential in SBGPTs is a multicriteria geospatial decision problem. We suggested three essential criteria for the evaluation of low-temperature resources (Figure 1):

- Geologic criteria (e.g., heat, accessible fluid, permeability, and seal).
- Economic criteria (e.g., population, infrastructure, heating and cooling demand, levelized cost of heat).
- Risk criteria (e.g., exclusion areas, and environmental/natural disaster regions).

The focus of this paper is exclusively on the geological criteria, our goal is to identify potential locations for more detailed geological data collection. Further work has been conducted to effectively integrate other criteria in the future.

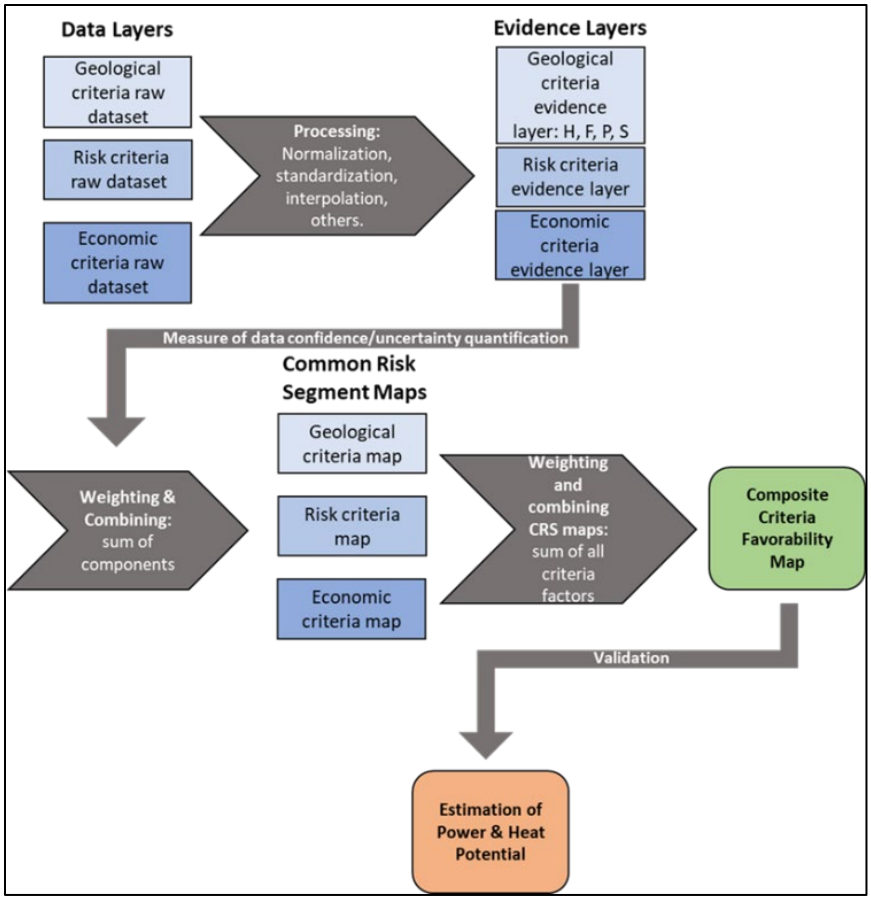

Figure 1: Flow chart outlining a generalized methodology for low-temperature assessment resources modified from Pauling et al. (2023) by Davalos-Elizondo et al. (2023)

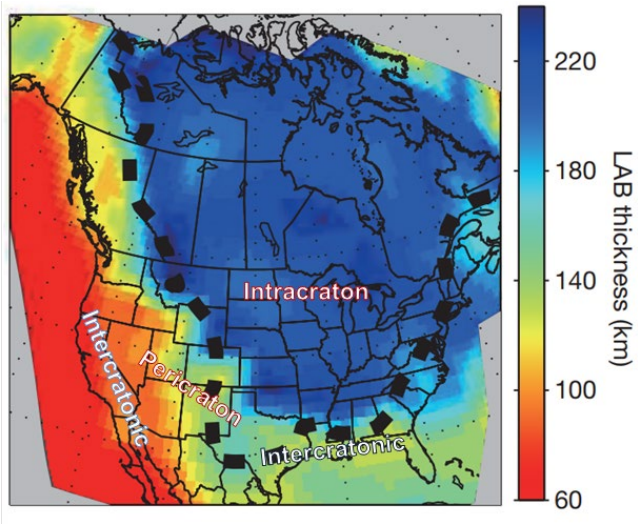

Figure 2: Present lithospheric-asthenospheric boundary thickness of North American continent from Yuan and Romanowicz (2010). A thick black dashed line indicates the borders of the craton

2. Background

The Denver Basin is characterized as a geothermal sedimentary foreland basin play type (Figure 3). This foreland basin is located on the eastern side of the Rocky Mountain orogenic belt in a pericratonic setting. Foreland basins are sedimentary basins that form between an orogenic belt and a craton, characterized by thick sedimentary deposits and asymmetric shape (Allen et al. 1986). They develop due to the weight of thickened crust and deposited sediments, causing the lithosphere to bend downward and create zones of extension and normal faulting. The formation of foreland basins is driven by factors such as horizontal compression, slab pull, lateral asthenospheric push, and delamination of the retreating mantle lithosphere (Garcia-Castellano and Cloetingh 2011). The rigidity of the plates also plays a key role in controlling the geometry and drainage history of foreland basins.

The Denver Basin is asymmetric, with suspected granite basement rocks underneath the sedimentary cover. It becomes much deeper as it stretches towards the Front Range in the western direction, reaching depths of around 3.5 km, while it is approximately 1.6 km deep in the eastern part (Dixon 2002). It spreads across more than 82,000-km^2 area, primarily in Colorado, followed by smaller portions in Wyoming and Nebraska (Fishman 2005). This basin is renowned for its petroleum extraction, with thousands of wells drilled for oil and gas production in various reservoir formations, providing data that describes the subsurface conditions.

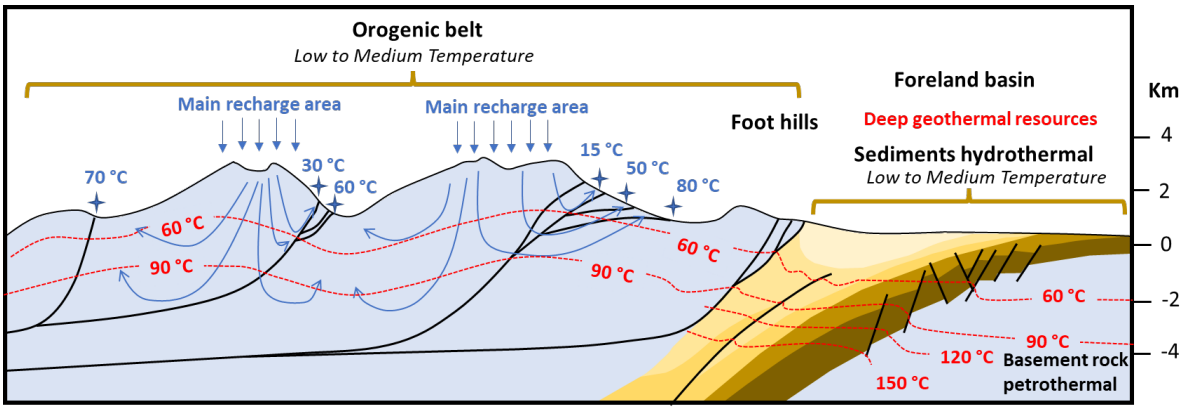

Figure 3: Orogenic Belt Geothermal Play Type and related SBGPT foreland basin. Modified from Moeck (2014)

3. Methodology

A classification of the Denver Basin geothermal play type as a foreland basin was established to outline the specific scope of work. Our approach includes: 1) identifying relevant data; 2) developing python code to combine multiple relevant data into PFA for geological criteria; and 3) rendering favorability or common criteria maps for low-temperature geothermal resources.

The PFA workflow was adapted accordingly (Figure 2) allowing overlaying of multiple geological criteria layers (see Table 1) to evaluate resource potential. We created favorability maps to identify suitable regions for CHP and GDU technologies. Moreover, the Python library titled “geoPFA” was developed and utilized to generate a workflow for producing common and composite maps

(Section 5). This Python library and its implementation are updated as the project and related work evolve, and it is expected to be released as an open-source toolset when it is robust enough.

QGIS, an open-source geographic information system from OSGeo, was used in combination with the geoPFA Python library to combine and process (e.g., interpolate, standardize, transform) different sets of geographic data related to the geological criteria from the raw data layers (e.g., heat, fluid, permeability).

The relevant data for this PFA workflow is outlined in Table 1, but may vary depending on data availability, region, and new discoveries.

Table 1. Relevant data suggested for PFA of low-temperature geothermal resources in the Denver Basin

GPT and Combination Method	Criteria	Component	Data
Pericratonic Foreland basin Modified Voter Veto	Geological	Heat	Bottom-Hole Temperatures
			Gradient Temperatures
			Thermal Conductivity
			Heat Flow
		Accessible Fluid	Hot Springs
			Co-production Water (BBL) Per Year
			Groundwater Wells
		Permeability	Faults and Shear Zone
			Earthquake Data

4. Relevant Data

4.1 Geological Criteria

Choosing optimal locations for low-temperature GHC and GDU opportunities involves the consideration of multiple factors. Suitability of sites is determined, in-part, based on geological criteria, such as heat, fluid, and permeability components (Section 3, Table 1). Combining these criteria into favorability maps suggests viable domains for low temperature geothermal resource utilization, without consideration for other important factors like risk and economic criteria.

4.1.1 Heat Component Analysis

Analyzing the temperature at the bottom of oil and gas wells, along with navigating limited certainty of reported bottom-hole temperature (BHT) accuracies, forms the basis for evaluating geothermal resources, according to Spicer (1964) and Whealton (2015, 2016). The end goal of our assessment is to determine the heat flow throughout the Denver Basin, suggesting areas of high heat flow that may be suitable for low-temperature geothermal resource utilization. There is a wealth of temperature data Python from oil and gas wells in the Denver Basin; decades of historic oil and gas production has provided many datapoints in the western and central regions of the Denver Basin. The basis for our heat component evaluation relies on BHT datasets as reference points for temperature at depth.

We identified three BHT datasets (Figure 4A): (1) Southern Methodist University (SMU); (2) Association of American State Geologists (AASG); and (3) Colorado Geological Survey (CGS). BHT data from Wyoming, Nebraska, and Colorado was gathered and narrowed down to focus specifically on the Denver Basin region. Despite abundance of BHT data, measurements can be distorted by heat changes caused by drilling and errors during data collection; for instance, if BHT data comes from a survey conducted a week after drilling, mud circulation could cause the BHT measurement to be falsely lower than if the data point were collected from a thermally stable shut-in well. Several correction methods have been created to estimate equilibrium conditions for BHTs in sedimentary basins (e.g., Harrison et al. 1983; Förster & Merriam 1995; Blackwell & Richards 2004).

To estimate heat flow and temperature distribution at depth, understanding the thermal conductivity of thousands of boreholes was necessary. It involves assigning lithologic units, unit thicknesses, and thermal conductivities from the surface to the basement for each borehole that had BHT data in the analysis. We utilized the lithology charts and thermal conductivity values used by the SMU data from AAPG COSUNA in the Denver Basin. To complete this assessment, an interpolation was performed, which estimated the likely distribution of thermal conductivity throughout the basin (Figure 4B). Higher thermal conductivities are associated with the southwest Denver Basin, while a nearly static thermal conductivity of 1.6 W/m/K is consistent in the northeast.

This project generated a uniformly corrected set of BHT datapoints from the SMU, AASG, and CGS datasets. Applying a generalized correction scheme was required. If a prior BHT correction scheme had been applied to the constituent datasets, that correction was reversed to obtain the original uncorrected BHT datapoints (i.e., AASG). We used the Förster correction to unify the datasets. The Förster correction has been suggested as the best correction scheme tailored for Denver Basin based on equilibrium data by Crowell et al. (2012; Equation 1):

$$Tcf = 0.0124\ x + 7.8825 \quad (1)$$

where Tcf is the temperature correction factor, and x is the depth at which the BHT measurement was reported. It is important to mention that this correction formula is only suitable for the Denver Basin and potentially other basins that have comparable stratigraphy (Crowell et al. 2012). For this reason, the Förster equation was applied to the Wyoming portion of the Denver Basin to the limited BHT datapoints in that region, as the stratigraphy is not drastically different from the Colorado and Nebraska portions (which the Förster correction scheme had been applied to previously in Crowell et al. 2012). The BHT data of SMU, AASGS, and CGS were corrected with the Förster equilibrium factor (Figure 5). Overall, the improved unified BHT dataset offered a more thorough evaluation of BHTs, reducing uncertainty and navigating potential errors in the datasets via tailored correction scheme for the Denver Basin. This unified BHT data will be available in the Geothermal Data Repository.

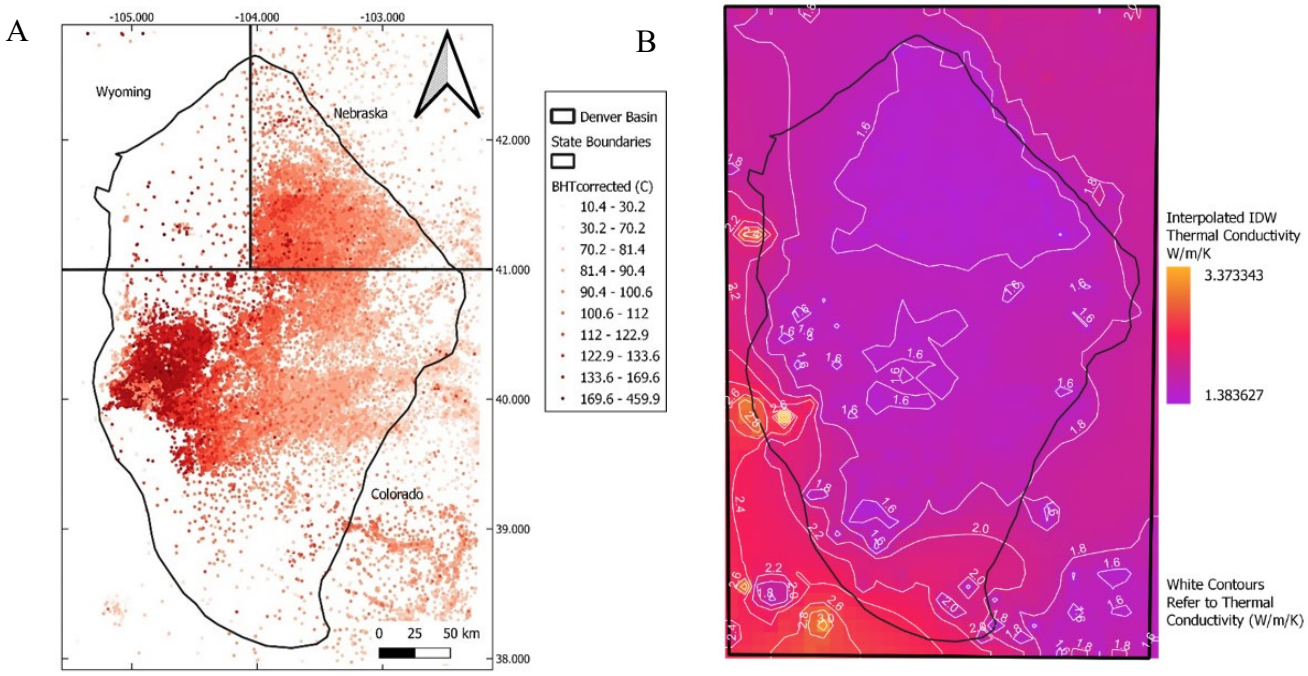

Figure 4: A. Bottom-hole temperatures of oil and gas wells in the Denver Basin from three different datasets: SMU, AASG, and CGS. Depth increases to the western side and decreases towards the eastern side of the basin. B. Thermal conductivities interpolation of rock across the Denver Basin

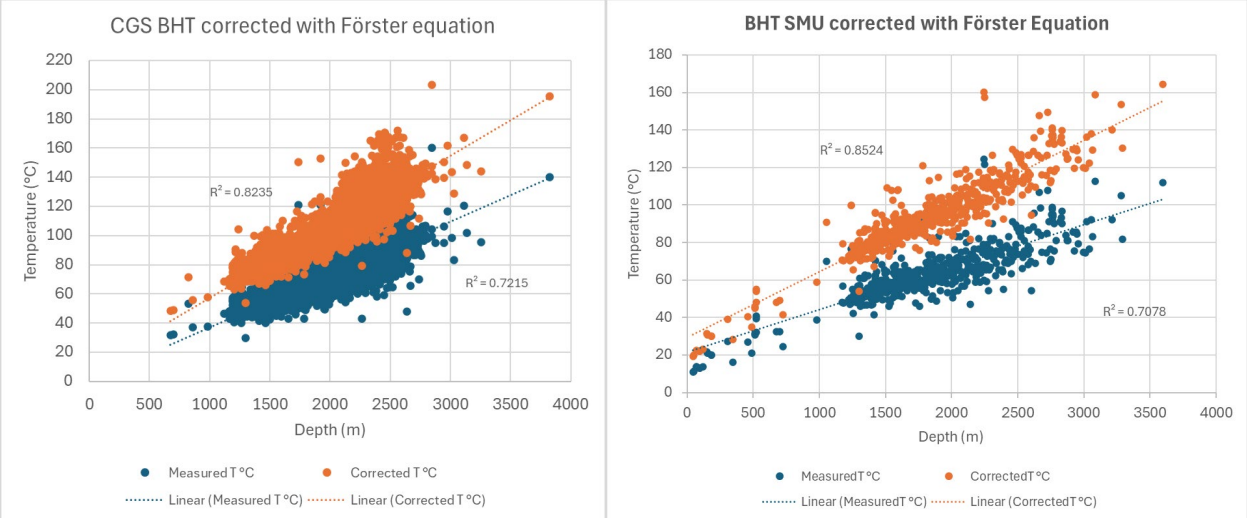

Figure 5: Bottom-hole temperature data of SMU and CGS corrected with the Förster equilibrium factor suggested by Crowell et al. (2012)

Heat transfer is also an essential factor in assessing the potential of geothermal resources, as the heat discharge data linked to Earth's heat flow is a vital indicator of potential. Heat flow maps are valuable tools for pinpointing regions of high geothermal resource potential in a specific area or country (Blackwell et al. 2007). The geothermal gradient plays a vital role in determining heat flow. Therefore, the uniformly corrected BHT dataset was used to estimate a temperature-depth profile (Figure 6A) in equilibrium developed by Crowell et al. (2012). We estimated the geothermal gradient as follows (Equation 2):

$$dT/dZ = [\text{corrected BHT datapoint} - \text{Surface temperature (°C)}]/ \text{depth (m)} \quad (2)$$

where dT/dz is the geothermal gradient (°C/Km).

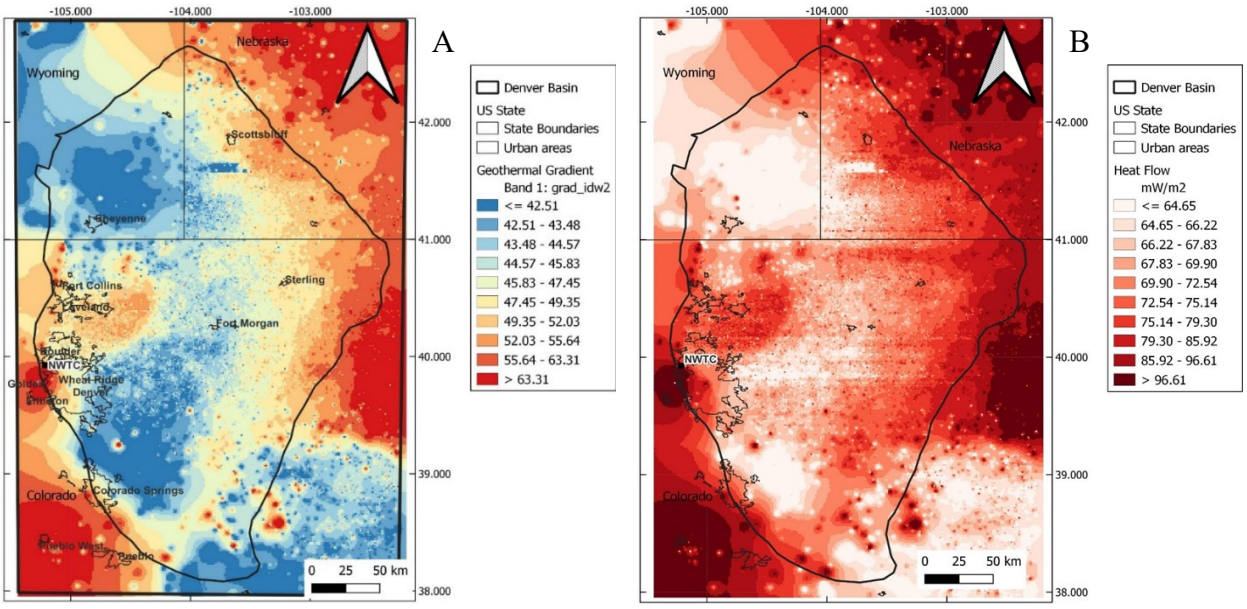

Figure 6: A. Geothermal gradient estimated from BHT data at 1 km. The average gradient temperature in the Denver Basin ranges around 42°C/km to 63°C/km. B. Heat Flow map of the Denver Basin calculated from geothermal gradient and thermal conductivities from SMU data. The heat flow map shows ranges around 64 to 96 mW/m^2. NWTC: National Wind Technology Center facility

We calculated heat flow as a function of depth (mW/m^2; Figure 6B). The uniform BHT dataset is required to estimate a geothermal gradient in conjunction with the lithology-dependent thermal conductivity. The following equation was used to estimate the heat flow:

$$Q = dT/dz * K \quad (3)$$

where Q is the heat flow (mW/m^2), dT/dz is the geothermal gradient (°C/Km), and K is thermal conductivity (W/m/ K), see Figure 4B.

The 1D heat flow model contains the following input assumptions and simplifications:

1. The model assumes that the generation of radiogenic heat is consistent and evenly spread throughout sedimentary rocks.
2. Input data was spatially interpolated to estimate the average and standard error of the average data values for the resource, producing maps depicting thermal quality in a GeoTIFF format (Figure 6).

In the Denver Basin, BHT data are concentrated in regions containing oil and gas reserves, such as central Colorado, while data are scattered in areas lacking exploration, such as southeastern Wyoming and southern Colorado. Sparsity of data in areas of the basin necessitates interpolation algorithms that can accurately predict nonexistent datapoints in both sparse and clustered datasets.

The intended application of the heat component is to suggest areas with a high geothermal resource potential based on temperature gradient as a proxy of heat flow, with high-temperature resources above 150°C typically used for generating electricity, while lower-temperature resources (<150°C) can be utilized for various direct applications such as heating buildings, industrial processes, agriculture, and recreational purposes.

4.1.2 Fluid Component Analysis

This first analysis was focused on the presence of coproduction water in oil and gas wells. Water production data can be used to provide information about where flowing water exists in the basin. It also indirectly provides a proxy for permeability aquifers and/or geothermal reservoirs, which is a key factor in hydrothermal resource and direct-use assessment. This type of data indicates reservoir quality of rocks by showcasing their capacity to uphold fluid flow rates needed for extracting heat from the rocks.

The main source for this water coproduction data from O&G wells in the Denver Basin is the USGS database that collates drilling and production records in the United States. The USGS dataset offers a comprehensive summary of the production records of U.S. wells spanning from 1817 to 2020. It was constructed using information gathered by IHS Markit, a commercial database provider. The production figures are consolidated in increments ranging from 2 to 10 square miles, detailing the cumulative output of oil, gas, and water volumes. In this study we used water production aggregated in 2 miles square that sum production per year in Barrels (BBL; Figure 7A).

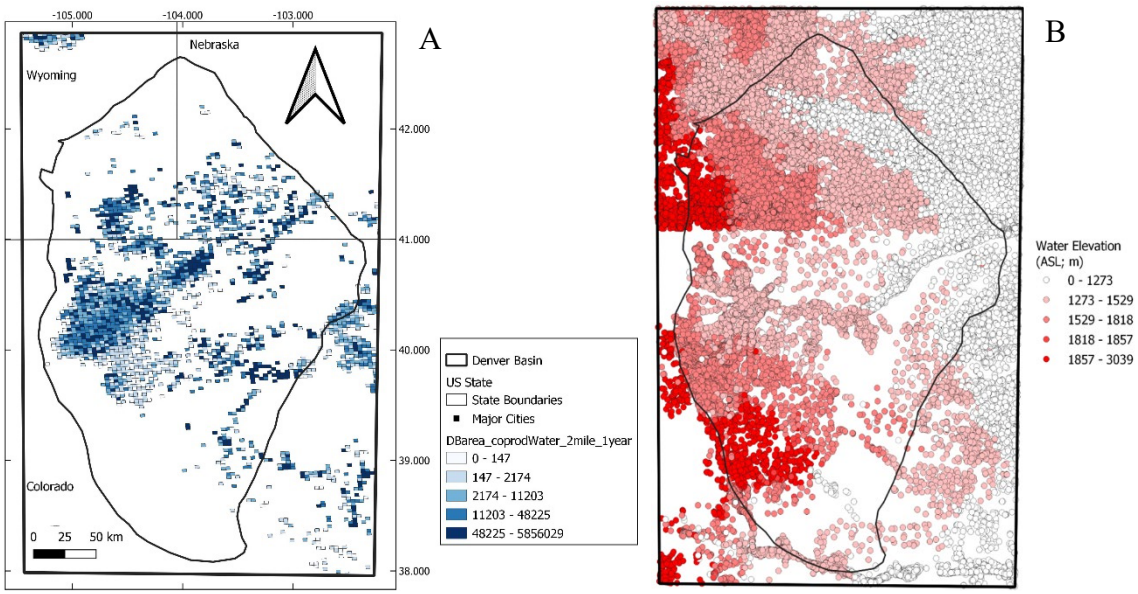

Figure 7: A. Water coproduction volumes (BBL) per year from oil and gas wells in the Denver Basin. B. Well water levels for Colorado, Nebraska, and Wyoming

The data quality information mentioned that comparing the annual production numbers with the total production figures revealed a discrepancy likely stemming from wells with unspecified production years. To ensure accuracy, the consistency between the original and processed total production values was verified. Moreover, a cross-check of well counts in various categories was

performed to confirm alignment, with the disparity between annual and total figures attributed to wells lacking spud dates.

Deeper reservoirs in the Denver Basin are well explored; for instance, over 8,000 wells have been drilled across the basin into the top of the Terry ("Sussex") sandstone alone (Fishman 2005). When investigating potential for direct-use geothermal energy (range of 50 m to 1,000 m vertical depth; minimum 80°C), grasping the potential volume of fluid available in shallower reservoirs is crucial. To achieve an estimation of shallow fluid availability, the elevation of static water level for all available groundwater wells in the Denver Basin area was calculated in Equation 4:

$$WL=GL-SWL \quad (4)$$

where WL (ft) is the water elevation in the well above sea level, GL (ft) is the ground surface elevation, and SWL (ft) is the reported static water level measured in the well. The datasets used to create an estimated water elevation in the Denver Basin were: SEO groundwater wells, where the depth to water (static water level) and well depth was reported in feet (WWDC 2024) and the ground elevation was obtained from USGS DEM files and converted to feet; CDSS wells, where the water elevation was reported as field 'WLElevation' in feet; and DNR for Nebraska, where Static Level was reported in feet. Well water elevation availability is visualized in Figure 7B.

4.1.3 Permeability Component Analysis

The permeability component analysis was simplified using structural geology data (e.g., faults and shear zones) and earthquake data due to a lack of accessibly data and short time frame to find, collect, and organize porosity, thickness, and other permeability data of reservoirs rock in the Denver Basin.

Most of the structural data in the region (Figure 8A) is inferred from surface fault features predominantly located in the western and southwestern parts of the Denver Basin. In the western section, the prevailing fault structures are primarily high-angle reverse faults that trend northwest and dip northeast, as documented by Erslev and Selvig in 1997. On a more specific level within the Wattenberg area, north of Denver, smaller but important structural characteristics are evident. These include ENE-trending wrench strike-slip faults and related listric normal faults with NNE, N, and NNW trends, as highlighted in works by Fishman (2005), Weimer (1996), and Weimer & Davis (1996). Research from multiple sources, such as Fishman (2005) and Weimer (1996), suggests the existence of five significant wrench faults in the Denver Basin within right-lateral movement along vertical planes, extending from the basement to the sedimentary cover (Weimer 1996). The intricate patterns of faulting indicate that the region is predominantly experiencing compressive stress, with the highest horizontal stress oriented towards the NNW, as noted by Heidbach et al. (2018).

Secondary permeability in the Denver Basin was assessed by distance from geologic structures in the Denver Basin. In a study conducted by Filina et al., structures in Nebraska were interpreted from a filtered magnetic field (2018). The structures identified in the study were digitized and included in the assessment of Denver Basin secondary permeability. Colorado structures were obtained from the USGS Geologic Map Database, and Wyoming structures were obtained from the Wyoming State Geological Survey. Primary permeability data of aquifers and rock formations were not accessible.

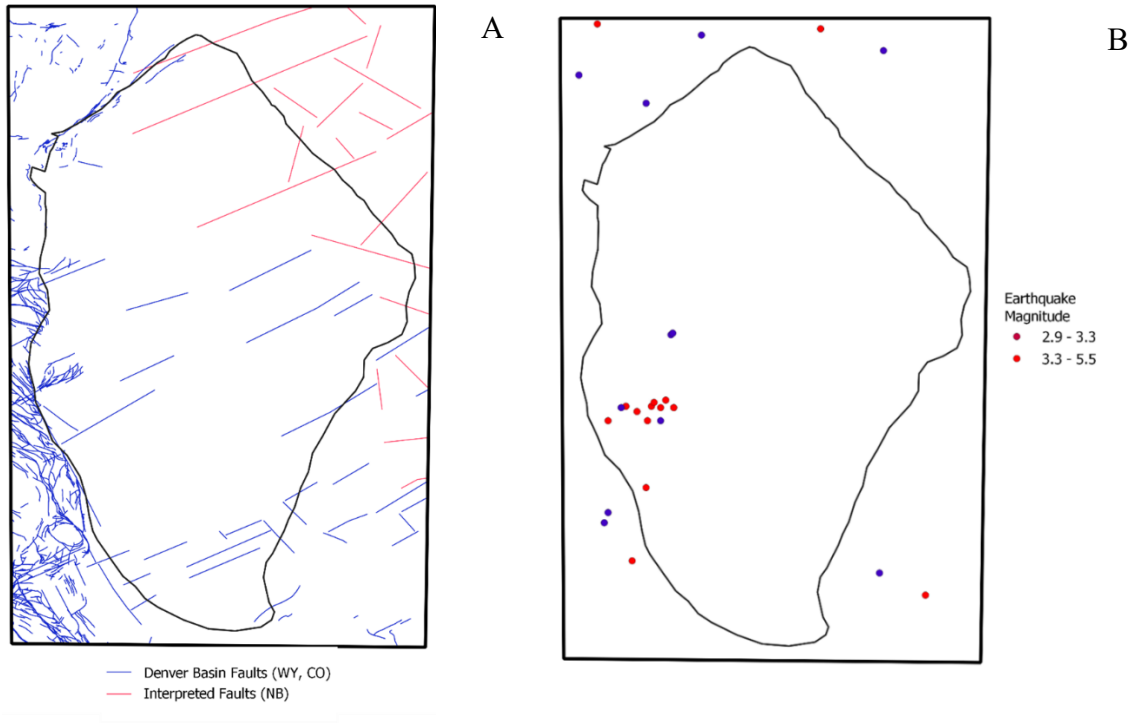

Figure 8: A. Faults and filtered magnetic lineaments and structures in the Great Basin area. B. Earthquakes greater than 2.9 magnitude in the Denver Basin from USGS earthquake catalog

To project secondary permeability of active faults, earthquake data from the 1950s to present day that was equivalent to or exceeded 2.9 magnitude was obtained from the USGS earthquake database presented in Figure 8B to identify Quaternary Faults and permeability of fluid pathways.

5. PFA Methodology

The Python library geoPFA was built with extensibility and reusability in mind, in the hopes that it may eventually be developed further and released as an open-source Python library. It is technologically agnostic and is modelled after the workflows described in the PFA Best Practices report. The library includes tools for:

- Reading in geospatial data in various formats (i.e., shapefile, TIFF, CSV).
- Cleaning the data (i.e., projecting onto the same CRS and grid, changing geometry type).
- Processing the data (i.e., distance function, various interpolation methods).
- Transforming the data (i.e., standardization, various methods for going from data values/data layers to favorability values/evidence layers).
- Weighting and combining the evidence layers (i.e., Voter-Veto method).
- Plotting the data and ouputs.

Throughout this section, examples of how the geoPFA Python library can be used to conduct PFA will be provided. The geoPFA is expected to be released as an open-source toolset in the future.

5.1 Configuration

There are several required inputs for each criterion and each component in the PFA process. These include component weights, component prior probabilities, evidence layer weights, and data layer transformation methods. In the full PFA, we will also add in criteria weights since there will be multiple criteria.

Component weights and component prior probabilities were assigned using expert opinion. Transformation methods were assigned based on a simple understanding of which relative relationship between data values and favorability (e.g., high values are more favorable = No transformation, or vice-versa = Negate). This could also be done more intelligently in the next PFA iteration. Evidence layer weights were also assigned using expert opinion and are set to 1.0 when there is only one evidence layer within a component (i.e., heat). Below are these parameters in tabular format for the geologic criteria only (Table 2).

geoPFA is built to be extensible to any possible combination of criteria, associated components, and data layers. It does so through requiring a configuration file that specifies the relationship between the data layers, respective components, and respective criteria. It also specifies the weights, units, data column names, and required transformation method for each data layer, and the prior probabilities associated with each component. Figure A.1 in the Appendix shows the configuration file for the geologic criteria only, in json format, compiling the information from Table 2 into a machine-readable format. Note that additional criteria may be added to the configuration file and formatted in a similar way.

Table 2: Table of component weights, component prior probabilities, evidence layers, evidence layer weights, and transformation methods applied. This table provides the basis for the configuration file shown in Figure A.1 in the Appendix.

Criteria	Component	Component weight*	Component Prior Probability	Evidence Layer Name	Evidence Layer Weight**	Transformation method
Geologic	Heat	0.40	0.65	Temperature Gradient	1.0	None
Geologic	Permeability	0.30	0.50	Structures (Faults)	0.50	Negate
Geologic	Permeability	0.30	0.50	Earthquakes	0.50	None
Geologic	Fluid	0.30	0.50	Hot Springs	0.5	Negate
Geologic	Fluid	0.30	0.50	Groundwater	0.2	Negate
Geologic	Fluid	0.30	0.50	Coproduced Fluid	0.3	None

*Note that the Voter-Veto method, as published in Ito et al. 2017, does not allow use of component weights. We have created a modified version of the Veto equation for combining component and criteria probabilities using weights.
**Note that the data layer weights are set to 1 when there is only one layer associated with a component.

It is also important that the data directory follows this same structure: there is a directory for each criteria, which contains subdirectories for each component, which each contain their respective data layers. The temperature gradient shapefile is named as described in the configuration file. Everything is also named as it is in the configuration file. This structure is demonstrated in Figure A.2 in the Appendix.

The configuration file is read into a Jupyter Notebook and stored as a Python dictionary named ‘pfa.’ This ‘pfa’ dictionary is updated throughout the process so that the entire PFA process is stored in a single data structure. This allows users to reference different parts of the PFA process throughout the workflow, for example, by comparing the original data layer to the final resulting favorability map or comparing the component favorability maps to the criteria favorability map.

5.2 Read in Data

The configuration and setup make it straightforward to read in the data (see Appendix: Figure A.3). Figure A.3 in the Appendix is a screenshot of the code which uses the ‘gather_data’ function from the ‘GeospatialData’ class in the geoPFA Python library. In this code snippet, we limit the data gathering only to shapefiles, but this can be adjusted to other formats, or all compatible geospatial data formats (currently shapefile, TIFF, and CSV). You can see from the text output that three data layers were read in–one for each component of the geologic criteria.

We can plot the raw data layers and see that they include various geometries (from left to right: point, line, and polygon), different CRSs, and different data spacing. The data need to be converted into point geometries, interpolated and/or processed to represent a feature of interest (e.g., distance from faults instead of fault traces), and projected onto the same CRS and the same grid (Figure 9). They also require some cleaning of outliers to show the trends more clearly in the data. These raw data layers are stored in Pandas GeoDataFrames (a type of dataframe that stores geospatial metadata and geometry) and added to 'data’ keys within their associated layer/component/criteria path within the ‘pfa’ dictionary so that they can be plotted at any point throughout the process.

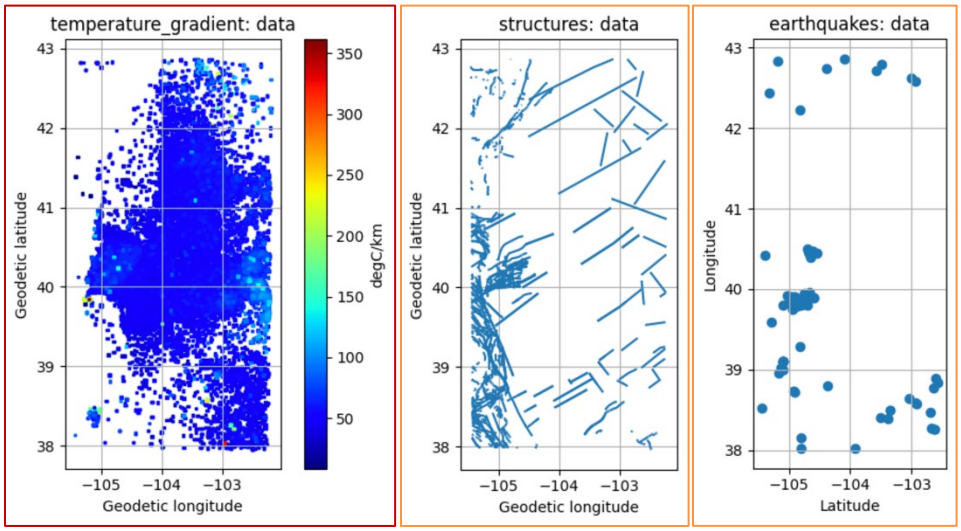

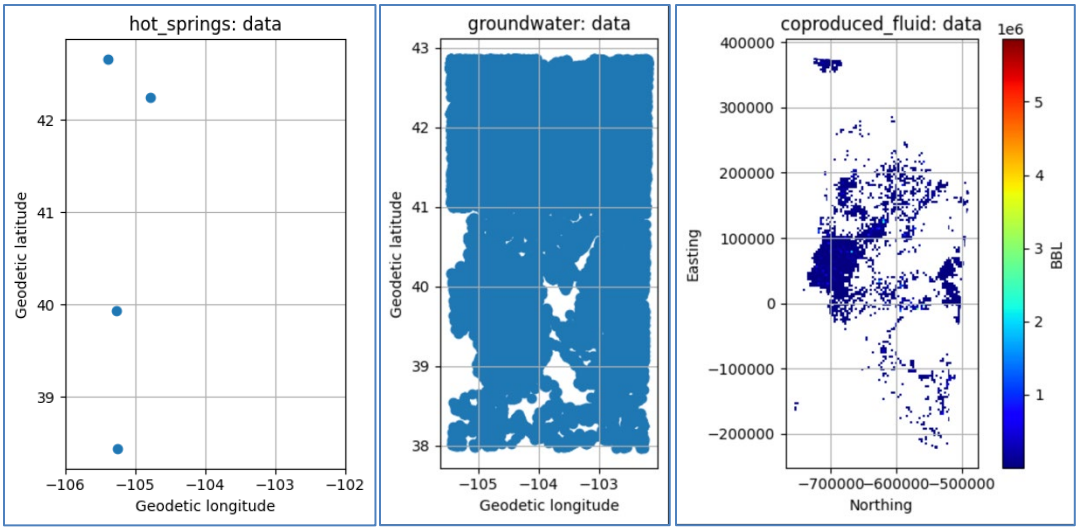

Figure 9: Raw data layers input into geoPFA for geologic criteria favorability mapping, including layers associated with the heat (red border), permeability (orange border), and fluid (blue border) components

5.3 Cleaning and Processing

Cleaning is done in just a few lines of code (Appendix: Figure A.4). This includes projecting everything onto the same CRS and filtering out outliers in some datasets by setting everything above the 0.9 quantile to the value associated with the 0.9 quantile. Particularly, the coproduced fluid and temperature gradient datasets included anomalously high values that masked the trends in the data. Outliers above the 90th percentile were filtered out and set to the value at the 90th percentile. Next, all the datasets were projected onto the same CRS. WGS 84 (EPSG:3857) was used because it is a common projected coordinate system. A projected coordinate system is a requirement for the interpolation and distance function to be accurate.

Linear interpolation is applied to temperature gradient and coproduced fluid data to produce 2D maps from these point datasets. A Euclidean distance function is used to calculate distance from faults, converting this line dataset into a 2D map. All three of the resulting 2D maps are on the same grid with the same CRS.

This is done using functions built into the 'Cleaners' class in the geoPFA. Currently the code requires somewhat manual cleaning of the data, but this could be automated in the future through allowing the user to specify cleaning methods for each layer within the configuration file.

Next, the data layers are interpolated/processed into maps (Appendix: Figure A.5). This process also puts all the layers onto the same grid through setting the 'nx,' 'ny,' and 'extent' variables. In addition, since the 'interpolate_points' function in the 'Processing' class of geoPFA requires point geometry, the polygon geometry of the produced fluid data layer is converted to point geometry by calculating the centroid of each grid square and applying the values for each grid square to its associated centroid. We have built this functionality into the 'interpolate_points' function. Currently, this function includes options for linear, cubic, or nearest-neighbor interpolation, and the linear option is selected.

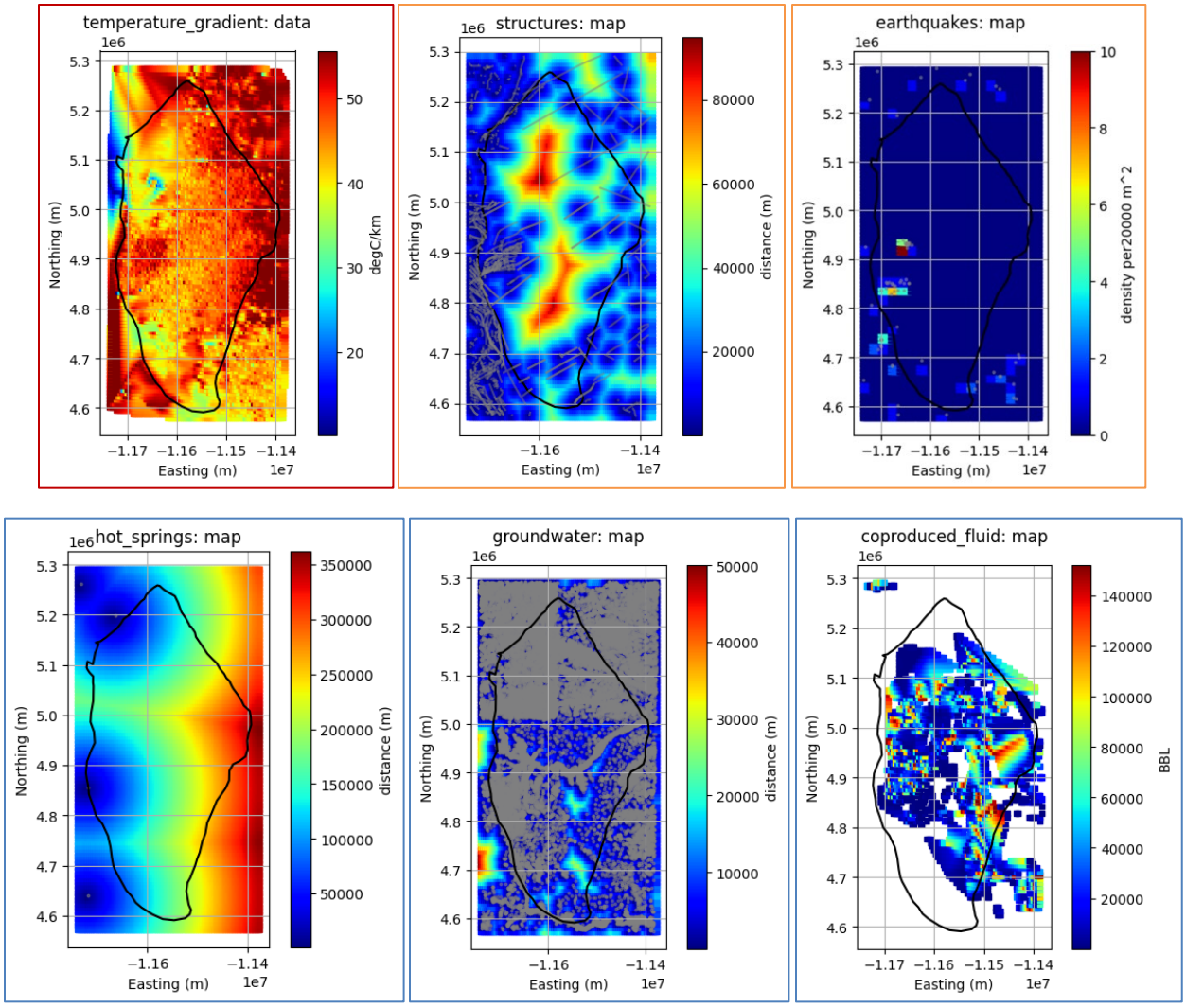

Figure 10: Processed data layers (or maps) input into geoPFA for geologic criteria favorability mapping, including layers associated with the heat (red border), permeability (orange border), and fluid (blue border) components Note that gray lines and dots represent data locations. Data locations are not labelled in the temperature gradient and coproduced fluid maps because the data points are dense and hide the trend in the interpolation

The fault location data is easily converted into a 'distance from faults' map using the 'distance_from_lines' function, and the hot springs and groundwater datasets are converted into 'distance from hot springs' and 'distance from groundwater observations' maps using the 'distance from points' function. The earthquake location data is converted into an 'earthquake density map' using the 'point_density' function. All three of these functions are in the 'Processing' class of the geoPFA. Similar to the cleaning functionality, geoPFA requires somewhat manual processing of the data, but this could also be automated in the future through allowing the user to specify processing methods for each layer within the configuration file.

The resulting maps are added to 'map' keys within their associated layer/component/criteria path within the 'pfa' dictionary so that they can be plotted at any point throughout the process. Above are the resulting maps produced from the processed data layers (Figure 10).

5.4 Transformation and Layer Combination

Next, all the data layers need to be converted into evidence layers. This involves normalizing and transforming (mapping data values to favorability values) each of the data layers. The evidence layers are then weighted and combined using the Voter-Veto method (Ito et al. 2017).

These steps are all built into the 'do_voter_veto' function in the VoterVeto class because transformation methods are specific to a given layer combination method. Transformation methods are additionally specific to a given data layer and are therefore specified in the configuration file for each data layer (Appendix: Figure A.6). For example, lower distance from faults is more favorable than higher distance from faults, so the evidence layer is produced by multiplying the fault distance map by –1 ('negate' method). No transformation methods are applied to the temperature gradient and coproduced fluids data layers because higher values are more favorable. In the future, transformation methods will be improved to better represent probability distributions associated with data layers as they pertain to their respective components and criteria. This will enable mapping of probabilities rather than just relative favorability.

Each data layer is normalized using min-max normalization. This puts all datasets on the same, positive, scale so that datasets with higher magnitudes do not dominate the results. Normalization may be done using either 'min-max' or mean absolute deviation ('mad').

Figure A.6 in the Appendix shows that we are able to normalize, transform, weight, and combine all of the data layers using just one line of code and the information (i.e., prior probabilities, transformation methods) stored in the configuration file. This uses the 'do_voter_veto' function from the 'VoterVeto' class in the geoPFA.

The 'do_voter_veto' function is written to complete the following steps:

1. Converts the data from a Pandas GeoDataFrame into a rasterized array to allow linear algebra/matrix math.
2. Transforms the data layers ('map') into evidence layers ('pr') using the transformation method specified for each data layer in the configuration file (if any) and then normalizing.
3. Weights and combines evidence layers into component favorability maps using the 'voter' method with the evidence layer weights in the configuration file.
4. Combines component favorability maps using the 'veto' method.
5. Combines criteria favorability maps using the 'veto' method.
6. Converts the rasterized favorability maps back into Pandas GeoDataFrames with the original geometry.

In other words, the weights and prior probabilities described in Table 2 are used in a modified version of the Voter-Veto equation (Ito et al., 2017). Within the Voter-veto method proposed by Ito et al, the Voter method (generalized linear model) is used to combine data layers into component favorability maps. Then, the modified Veto equation (element-wise multiplication) is used to combine component favorability maps into a geologic criteria favorability map, and to combine criteria maps into combined overall favorability maps, vetoing areas where any component criteria have a favorability value of 0. The original equations for this methodology are

described in Section 2.1 of Ito et al., 2017, and our modified version of the Veto equation is as follows:

$$\Pr(R) = \frac{\sum^c w_c \Pr(X_c)}{\max[\sum^c w_c \Pr(X_c)]} \times \max[\prod^c \Pr(X_c)] \quad (5)$$

where PrR is the probability of a resource, w_c is the weight of a given component or criteria, and Pr(X_c) is the probability of a given component or criteria. In written language, the equation produces a weighted some of the components or criteria, depending on which level the probability mapping is occurring on, normalizes by dividing by the maximum value, and scales using the product of the individual component or criteria probability maps to ensure that the resulting probability map represents a valid probability distribution. The veto portion of the equation is optional, but when desired, resulting indices in Pr(R) are set to zero if the associated indices in any Pr(X_c) are zero. In the methodology presented here, the veto option is used when combining criteria, but not when combining components.

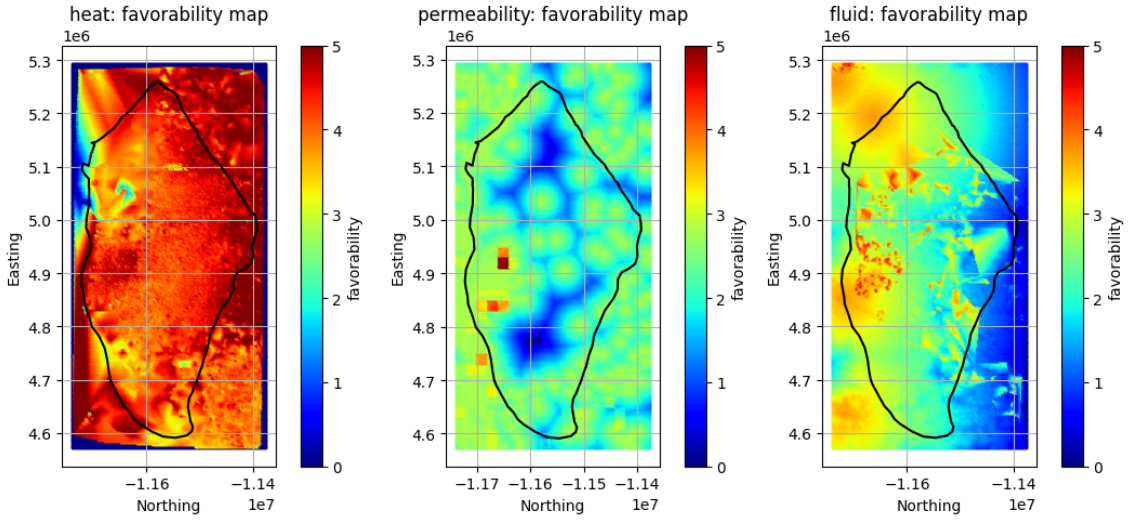

Figure 11: Geologic criteria component favorability maps, including heat, permeability, and fluid components, produced using geoPFA

The resulting evidence layers and component favorability maps are added to 'fav' keys within their associated criteria/component/layer and criteria/component paths, respectively, within the 'pfa' dictionary so that they can be plotted at any point throughout the process. The resulting component favorability maps are shown in Figure 11. Note that since we only are inputting one data layer to map the heat component, the temperature gradient evidence layer is equivalent to heat component favorability map, but typically this is not the case. The resulting criteria favorability maps are added to 'fav' keys within their associated criteria paths (in this case 'geologic') within the 'pfa' dictionary, and the resulting combined favorability map (not yet generated) is stored under a 'fav' key at the top level of the 'pfa' dictionary. The draft geologic criteria favorability map produced by geoPFA is shown in Figure 12.

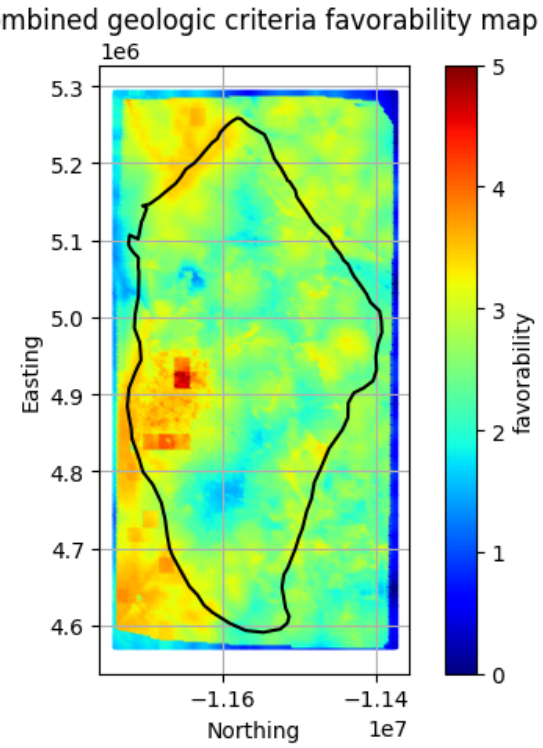

Figure 12: Combined geologic criteria favorability map of the Denver Basin, produced using geoPFA

6. Geological Criteria Favorability Map

The resulting favorability map is shown below in Figure 13. In the future, more robust data transformation methods will be implemented to more realistically map data values to probability values.

The map appears to validate the methodology thus far. The map highlights the area to the west end of the Denver Basin (e.g., Wattenberg area) where there appears to be intersection between faults, some seismic activity, elevated temperature gradient values, ground water presence, a hot spring, and relatively high volumes of coproduced fluids. It also highlights some other smaller areas that are not as obvious to the human eye, within the northwest (in southeast Wyoming) and southwest areas (near Colorado Springs) of the Denver Basin.

However, the significant reliance on earthquake density as a component of permeability in the geothermal favorability map raises concerns about potential artifacts, as the highest probability area coincides with multiple back-to-back earthquakes in very close proximity to each other. This suggests that the earthquake component may need to be weighted lower in our future analyses to avoid artifacts in the resulting favorability maps.

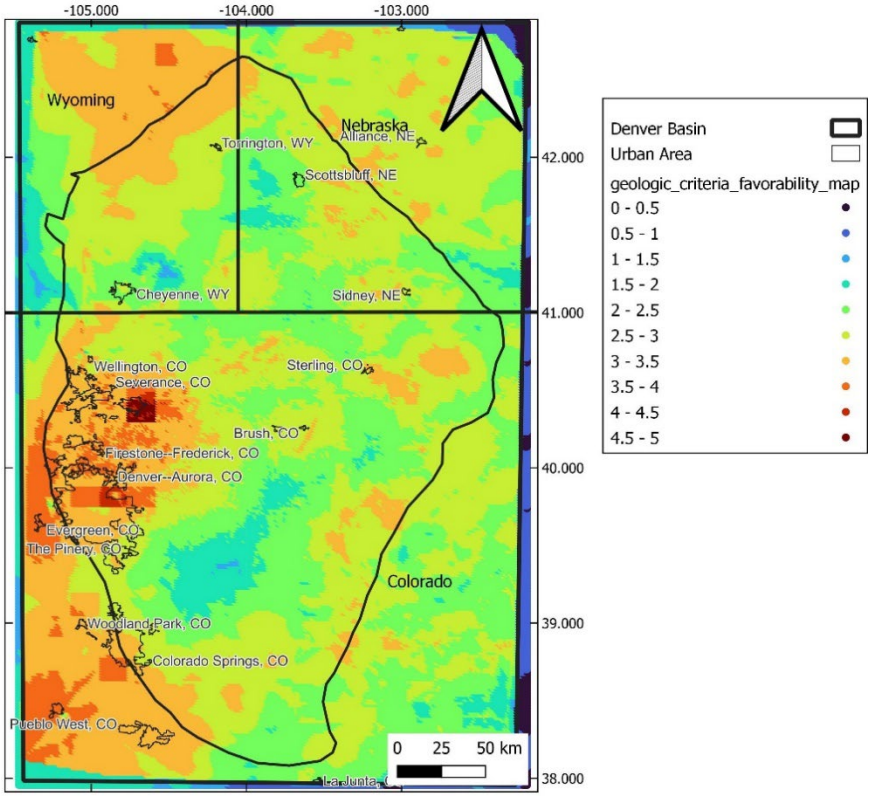

Figure 13: Geological Criteria Favorability Map for the Denver Basin

7. Conclusions

The study adapted PFA methodologies from previous studies to SBGPT to assess the potential of low-temperature resources in the Denver Basin. The resulting favorability map highlights areas with high potential for geothermal technology opportunities. While the map is still uncertain, it suggests promising areas, particularly in the western part of the Denver Basin.

To improve the accuracy and uncertainty quantification of the geological resource maps, future steps include: (1) incorporating additional high-quality data that provide enough information to create confidence layers; (2) adding more layers to the permeability component, particularly those that provide information about primary permeability in the geological formations rather than only secondary permeability; (3) improving interpolations and implementing more intelligent transformation methods; (4) refining prior probabilities and weights for each component (e.g., earthquakes will be weighted lower); and (5) building other layer combination methods into the geoPFA library, such as weights of evidence. The geoPFA Python library is expected to be released as an open-source tool in the future to enable others to use this code for their own PFA studies.

Furthermore, identifying potential areas for geothermal direct uses, and combined heat and power is a complex geospatial decision-making problem that requires consideration of multiple criteria. This paper was focused on the geological criteria, including heat, accessible fluid, and permeability, as essential factors for evaluating low-temperature resources. However, it is recognized that other critical criteria such as risk (seismicity, exclusion areas, and environmental/natural disaster) and economic factors (population, infrastructure, heating and

cooling demand, and levelized cost of heat) must also be considered in the evaluation process in this project. Future work will integrate these additional criteria to provide a comprehensive assessment of potential areas for geothermal applications.

In conclusion, this project aims to accelerate the country's decarbonization efforts by identifying opportunities for utilizing low-temperature geothermal resources (<150°C) in sedimentary basins with numerous population centers geothermal direct uses, and combined heat and power applications. The project has provided PFA workflows, data, tools, and favorability maps to support the utilization of low-temperature geothermal resources in the Denver Basin. Future improvements will focus on refining the methodology to ensure accurate and reliable results, ultimately facilitating future assessment of low-temperature geothermal resources in sedimentary basins and supporting the country's transition to a low-carbon economy.

Acknowledgement
This work was authored by the NREL operated by Alliance for Sustainable Energy, LLC, for the U.S. Department of Energy (DOE) under Contract No. DE-AC36-08GO28308. Funding and feedback provided by the U.S. Department of Energy Office of Energy Efficiency and Renewable Energy Geothermal Technologies Office. The views expressed herein do not necessarily represent the views of the DOE or the U.S. Government. The U.S. Government retains and the publisher, by accepting the article for publication, acknowledges that the U.S. Government retains a nonexclusive, paid-up, irrevocable, worldwide license to publish or reproduce the published form of this work, or allow others to do so, for U.S. Government purposes.

REFERENCES

Allen, P. A., Homewood, P. and Williams, G. D. 1986. Foreland basins: an introduction. In: Foreland Basins. Eds: P. A. Allen and P. Homewood, Special Publication of the International Association of Sedimentologists, 8, 3-12.

Augustine, C., 2014. Analysis of sedimentary geothermal systems using an analytical reservoir model. Geothermal Resources Council Transactions, 38, pp.641-647.

Blackwell, D. D., and Richards, M., 2004, Calibration of the AAPG Geothermal Survey of North America BHT Data Base: American Association of Petroleum Geologists Annual Meeting 2004, Dallas, Texas, Poster session, paper 87616.

Blackwell, D.D., Negraru, P.T. and Richards, M.C., 2007. Assessment of the enhanced geothermal system resource base of the United States. Natural Resources Research, 15, pp.283-308.

Coleman Jr, J.L. and Cahan, S.M., 2012. Preliminary catalog of the sedimentary basins of the United States.

Crowell, A.M., Ochsner, A.T. and Gosnold, W., 2012. Correcting bottom-hole temperatures in the Denver Basin: Colorado and Nebraska. GRC Transactions, 36(GRC1030229).

Davalos-Elizondo, E., Kolker, A., Taverna, N. and Holt, E., 2023. Assessing Low-Temperature Geothermal Play Types: Relevant Data and Play Fairway Analysis Methods (No. NREL/TP-5700-87259). National Renewable Energy Laboratory (NREL), Golden, CO (United States).

Dixon, J. M. (2002). Evaluation of Bottom-Hole Temperatures in the Denver and San Juan Basins of Colorado: Colorado Geological Survey.

Doughty, C., Dobson, P.F., Wall, A., McLing, T. and Weiss, C., 2018. GeoVision analysis supporting task force report: exploration.

Erslev, E.A. and Selvig, B., 1997. Thrusts, backthrusts and triangle zones: Laramide deformation in the northeastern margin of the Colorado Front Range.

Filina, I., Searls, M., Guthrie, K. and Burberry, C.M., 2018. Seismicity in Nebraska and adjacent states: The historical perspective and current trends.

Fishman, N. S. (2005). Energy Resource Studies, Northern Front Range, Colorado: US Geological Survey.

Förster, A., Merriam, D.F., and Davis, J.C., 1996, Statistical analysis of some bottom-hole temperature (BHT) correction factors for the Cherokee Basin, southeastern Kansas: Tulsa Geol. Soc. Trans., pp. 3-9.

Garcia-Castellanos, D. and Cloetingh, S.I.E.R.D., 2011. Modeling the interaction between lithospheric and surface processes in foreland basins. Tectonics of Sedimentary Basins: Recent Advances, pp.152-181.

Harrison W. E., Luza, K.V., Prater, M. L., and Chueng, P. K., 1983, Geothermal resource assessment of Oklahoma, Oklahoma Geological Survey, Special Publication 83-1.

Hartmann, D.J., Beaumont, E.A. and Coalson, E., 2000. Prediction sandstone reservoir system quality and example of petrophysical evaluation. Search and discovery, 40005.

Heidbach, O., Rajabi, M., Cui, X., Fuchs, K., Müller, B., Reinecker, J., . . . Xie, F. (2018). The World Stress Map database release 2016: Crustal stress pattern across scales. Tectonophysics, 744, 484-498.

Ito, G., Frazer, N., Lautze, N., Thomas, D., Hinz, N., Waller, D., Whittier, R., Wallin, E. (2017) "Play fairway analysis of geothermal resources across the state of Hawaii: 2. Resource probability mapping." Geothermics, Volume 70, 2017, Pages 393-405, ISSN 0375-6505, https://doi.org/10.1016/j.geothermics.2016.11.004.

Moeck, I.S., 2014. Catalog of geothermal play types based on geologic controls. Renewable and Sustainable Energy Reviews, 37, pp.867-882.

Moghaddam, M.K., Noorollahi, Y., Samadzadegan, F., Sharifi, M.A., Itoi, R., (2013) "Spatial data analysis for exploration of regional scale geothermal resources." Journal of Volcanology and Geothermal Research, Volume 266, Pages 69-83, ISSN 0377-0273, https://doi.org/10.1016/j.jvolgeores.2013.10.003.

Pauling, H., Taverna, N., Trainor-Guitton, W., Witter, E., Kolker, A., Warren, I., Robins, J., and Rhodes, G. (2023). "Geothermal Play Fairway Analysis Best Practices. Golden, CO: National Renewable Energy Laboratory." NREL/TP-5700- 86139. https://www.nrel.gov/docs/fy23osti/86139.pdf.

Rybach, L., 1981. Geothermal systems, conductive heat flow, geothermal anomalies. Geothermal Systems: Principles and case histories, pp.3-36.

Skinner, C.C., Miller, R.F., Kinney, S.A., Gianoutsos, N.J., Gunther, G.L., and Shorten, C.M., 2022, Aggregated Oil and Natural Gas Drilling and Production History of the United States (ver. 1.1, April 2023): U.S. Geological Survey data release, https://doi.org/10.5066/P9UIR5HE.

Spicer, H. C. (1964). A compilation of deep earth temperature data, U. S. A. 1910-1945. Open-File Report 64-167, U.S Geological. Survey.

USGS (2022) USGS CO2Viewer. Accessed from: https://co2public.er.usgs.gov/viewer/%0A

Weimer, P. and Davis, T.L. eds., 1996. Applications of 3-D seismic data to exploration and production (Vol. 5). Published jointly by the American Association of Petroleum Geologists and the Society of Exploration Geophysics.

Weimer. (1996). Guide to the petroleum geology and Laramide Orogeny, Denver Basin and Front Range, Colorado: Colorado Geological Survey Bulletin 51. Two miners inside the Black Diamond Mine (2).

Whealton, C. (2015). Statistical Correction of Temperature Data for New York and Pennsylvania Wells. M.S. Thesis, Cornell University, Ithaca. Retrieved from http://hdl.handle.net/1813/40609

Whealton, C. A. (2016). Statistical Data Analysis, Global Sensitivity Analysis, and Uncertainty Propagation Applied to Evaluating Geothermal Energy in the Appalachian Basin, in Ithaca, NY, USA, Cornell University, Ph.D. dissertation, p. 250

Wolfgramm, M., Obst, K., Beichel, K., Brandes, J., Koch, R., Rauppach, K. and Thorwart, K., 2009. Produktivitätsprognosen geothermischer aquifere in Deutschland. Der Geothermiekongress, pp.17-19.

Wyoming Water Development Commission, 2024. Groundwater water wells database. Accessed from: https://water.geospatialhub.org/pages/wwdc-gis-standards

Yuan, H. and Romanowicz, B., 2010. Lithospheric layering in the North American craton. Nature, 466(7310), pp.1063-1068.

Zimmermann, G., Reinicke, A., Blöcher, G., Milsch, H., Gehrke, D., Holl, H.G., Moeck, I., Brandt, W., Saadat, A. and Huenges, E., 2007, January. Well path design and stimulation treatments at the geothermal research well GtGrSk4/05 in Groß Schönebeck. In Proceedings Thirty-Second Workshop on Geothermal Reservoir Engineering (pp. 22-24). Stanford University Stanford, California.

APPENDIX A. Screenshots of code using geoPFA Python library

```
"criteria": {
    "geologic": {
        "weight": 0.35,
        "components": {
            "heat": {
                "weight": 0.4,
                "layers": {
                    "temperature_gradient": {
                        "weight": 1,
                        "units": "degC/km",
                        "data_col": "Gradient",
                        "transformation_method": "none",
                        "processing_method": "interpolate"
                    }
                },
                "pr0": 0.65
            },
            "permeability": {
                "weight": 0.3,
                "layers": {
                    "structures": {
                        "weight": 0.5,
                        "units": "NA",
                        "data_col": "None",
                        "transformation_method": "negate",
                        "processing_method": "distance"
                    },
                    "earthquakes": {
                        "weight": 0.5,
                        "units": "NA",
                        "data_col": "None",
                        "transformation_method": "none",
                        "processing_method": "density"
                    }
                },
                "pr0": 0.5
            },
            "fluid": {
                "weight": 0.3,
                "layers": {
                    "hot_springs": {
                        "weight": 0.5,
                        "units": "NA",
                        "data_col": "None",
                        "transformation_method": "negate",
                        "processing_method": "distance"
                    },
                    "groundwater": {
                        "weight": 0.2,
                        "units": "NA",
                        "data_col": "None",
                        "transformation_method": "negate",
                        "processing_method": "distance"
                    },
                    "coproduced_fluid": {
                        "weight": 0.3,
                        "units": "BBL",
                        "data_col": "SUM_WATER_",
                        "transformation_method": "none",
                        "processing_method": "interpolate"
                    }
                },
                "pr0": 0.5
            }
        }
    },
```

Figure A.1: Configuration file used to map criteria to components, components to data layers, and additional information to data layers. This configuration file is part of the required setup for geoPFA

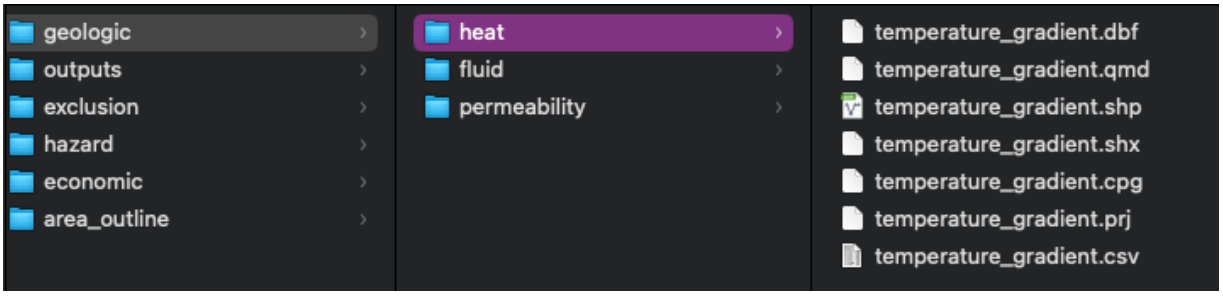

Figure A.2: Example directory structure for input data layers for geoPFA

Read in Data

```
file_types = ['.shp']
pfa = GeospatialDataReaders.gather_data(DATA_DIR,pfa,file_types)
```

```
criteria: geologic
        component: heat
                reading layer: temperature_gradient
        component: permeability
                reading layer: structures
                reading layer: earthquakes
        component: fluid
                reading layer: hot_springs
                reading layer: groundwater
                reading layer: coproduced_fluid
criteria: economic
        component: demand
                reading layer: population
                reading layer: infrastructure
        component: site_accessibility
                reading layer: roads
criteria: hazard
        component: natural_disaster
                reading layer: flood_plains
```

Figure A.3: Screenshot of code to read in data using geoPFA

Cleaning

```
pfa = Cleaners.set_crs(pfa, target_crs=3857)
```

```
data = pfa['criteria']['geologic']['components']['fluid']['layers']['coproduced_fluid']['data']['SUM_WATER_']
filtered_data = Cleaners.filter(data,quantile=0.9)
pfa['criteria']['geologic']['components']['fluid']['layers']['coproduced_fluid']['data']['SUM_WATER_'] = filtered_data
```

```
•••
```

```
data = pfa['criteria']['geologic']['components']['heat']['layers']['temperature_gradient']['data']['Gradient']
filtered_data = Cleaners.filter(data,quantile=0.9)
pfa['criteria']['geologic']['components']['heat']['layers']['temperature_gradient']['data']['Gradient'] = filtered_data
```

```
•••
```

```
gdf = pfa['criteria']['economic']['components']['demand']['layers']['population']['data']
clipped_gdf = Cleaners.set_extent(gdf,extent)
pfa['criteria']['economic']['components']['demand']['layers']['population']['data'] = clipped_gdf
```

```
gdf = pfa['criteria']['economic']['components']['demand']['layers']['population']['data']
col = pfa['criteria']['economic']['components']['demand']['layers']['population']['data_col']
filtered_gdf = Cleaners.filter_geodataframe(gdf,col,quantile=0.9)
pfa['criteria']['economic']['components']['demand']['layers']['population']['data'] = filtered_gdf
```

Figure A.4: Screenshot of code to clean data using geoPFA, including setting the CRS and filtering datasets

Interpolation

```
nx = 100; ny = 100
method = 'linear'
pfa = Processing.interpolate_points(pfa, criteria='geologic', component='heat',
                                    layer='temperature_gradient',
                                    interp_method=method,nx=nx,ny=ny,extent=extent)

method = 'linear'
pfa = Processing.interpolate_points(pfa, criteria='geologic', component='fluid',
                                    layer='coproduced_fluid',
                                    interp_method=method,nx=nx,ny=ny,extent=extent)
```

```
Notice: interpolate_points() function recieved GeoDataFrame with geometry type 'Polygon.'
Converting geometry to 'Point' geometry using centroids.
```

Distance Function

```
pfa = Processing.distance_from_lines(pfa,criteria='geologic',component='permeability',
                                     layer='structures',extent=extent,nx=nx,ny=ny)
pfa = Processing.distance_from_points(pfa,criteria='geologic',component='fluid',
                                     layer='hot_springs',extent=extent,nx=nx,ny=ny)
pfa = Processing.distance_from_points(pfa,criteria='geologic',component='fluid',
                                     layer='groundwater',extent=extent,nx=nx,ny=ny)
```

Density Function

```
cell_size = 80000
pfa = Processing.point_density(pfa, criteria='geologic', component='permeability',
                               layer='earthquakes', extent=extent, cell_size=cell_size,
                               nx=nx, ny=ny)
```

Figure A.5: Screenshot of code to process data using geoPFA, including interpolation, distance, and density functionalities

Transformation & Layer Combination

Combine layers from each component into component probability maps, and then resource probability maps, using the voter-veto method

```
pfa = VoterVeto.do_voter_veto(pfa,normalize_method='minmax',component_veto=False,criteria_veto=True)
```

```
Normalized a layer using minmax
Transformed a layer using negate
Normalized a layer using minmax
Normalized a layer using minmax
Transformed a layer using negate
Normalized a layer using minmax
Transformed a layer using negate
Normalized a layer using minmax
Normalized a layer using minmax
Normalized a layer using minmax
Normalized a layer using minmax
Transformed a layer using negate
Normalized a layer using minmax
Normalized a layer using minmax
```

Figure A.6: Screenshot showing code to transform and combine data layers in one line of code using geoPFA